Supporting Information for

TlP_5: An unexplored direct band gap 2D semiconductor with ultra-high carrier mobility

Jun-Hui Yuan,[1] Alessandro Cresti,[2] Kan-Hao Xue,[1,2*] Ya-Qian Song,[1] Hai-Lei Su,[1] Li-Heng Li,[1] Nai-Hua Miao,[3#] Zhi-Mei Sun,[3] Jia-Fu Wang,[4] Xiang-Shui Miao[1]

[1]Wuhan National Research Center for Optoelectronics, School of Optical and Electronic Information, Huazhong University of Science and Technology, Wuhan 430074, China

[2]Univ. Grenoble Alpes, Univ. Savoie Mont Blanc, CNRS, Grenoble INP, IMEP-LAHC, 38000 Grenoble, France

[3]School of Materials Science and Engineering, Beihang University, Beijing 100191, China

[4]School of Science, Wuhan University of Technology, Wuhan 430070, China

*Correspondence and requests for materials should be addressed to K.-H. Xue and N.-H. Miao (Email: xkh@hust.edu.cn; nhmiao@buaa.edu.cn)

First of all, we have checked the stability of bulk TlP_5 through the phonon dispersion calculation. The result in **Figure S1** shows only real modes, indicating good dynamic stability.

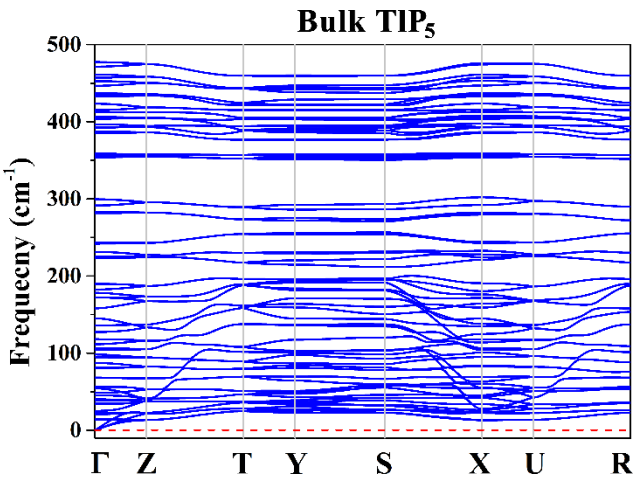

Figure S1 Calculated phonon dispersion relation of bulk TlP_5.

The phosphorus network founded in TlP_5 is very similar to the one observed in the monoclinic modification of red phosphorus, the so-called Hittorf's phosphorus.[1] As shown in **Figure S2**, in TlP_5 there are discernable tubes with pentagonal cross-sections, which are very characteristic structure of the phosphorus element in Hittorf's phosphorus. Comparing these two structures, one finds that the phosphorus network in TlP_5 can be regarded as stemming from a partial breaking of the network in Hittorf's phosphorus, as shown in **Figure S3.**

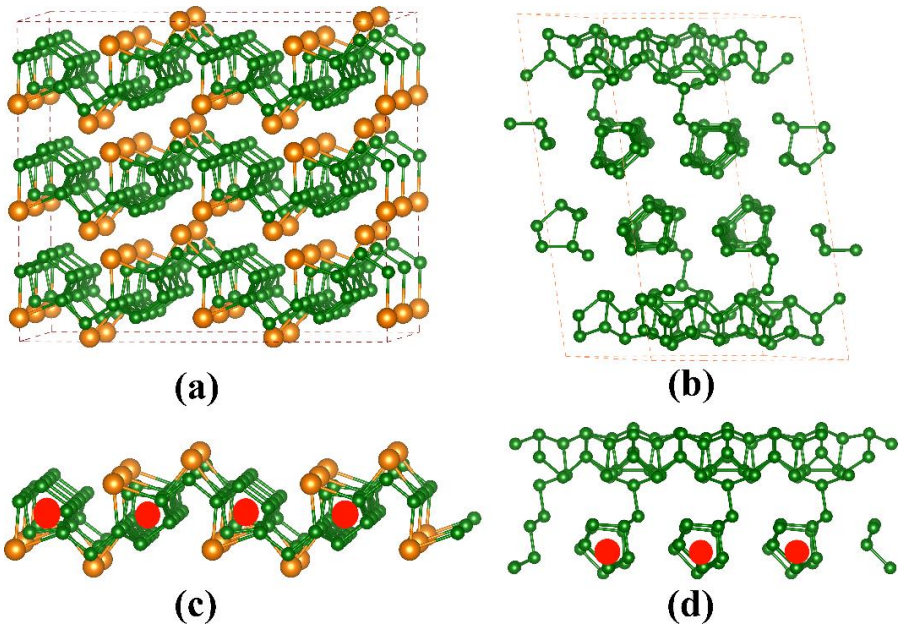

Figure S2 Demonstration of the crystal structures for: (a) bulk (2×3×2 supercell) TlP_5; (b) bulk (1×2×1 supercell) Hittorf's phosphorus; (c) monolayer (2×2×1 supercell) TlP_5; and (d) monolayer (2×2×1 supercell) Hittorf's phosphorus.

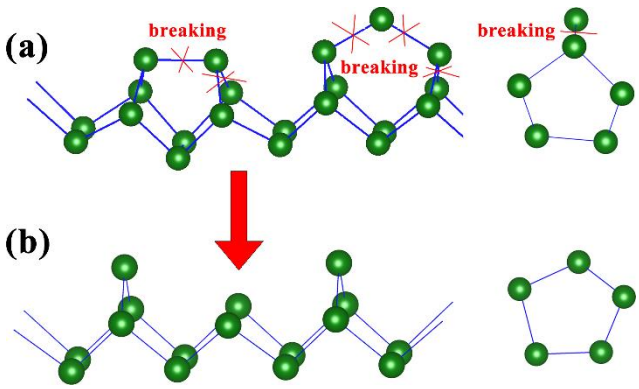

Figure S3 Comparison of the pentagonal tubes in the phosphorus network of (a) Hittorf's phosphorus and (b) TlP_5. Illustrations of the possible P-P bond breaking schemes are also given.

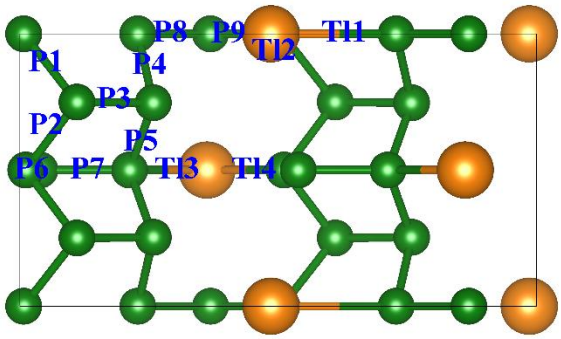

Figure S4 A schematic diagram of the P-P bonds and Tl-P bonds in monolayer and bulk TlP_5. Only a single formula unit of TlP_5 has been marked.

The bond lengths of P-P and Tl-P in both monolayer and bulk TlP_5 are listed in Table S1, together with the experimental results for the sake of comparison. The P-P bond lengths of monolayer TlP_5 are around 2.16 Å ~2.27 Å, while those of Tl-P are around 3.0 Å ~3.17 Å. These values are very close to those of optimized bulk TlP_5 (2.15 Å~2.28 Å for P-P bonds and 3.00 Å~3.09 Å for Tl-P bonds). Most of the P-P and Tl-P bond lengths in monolayer TlP_5 are slightly larger than in the bulk, which is as expected.

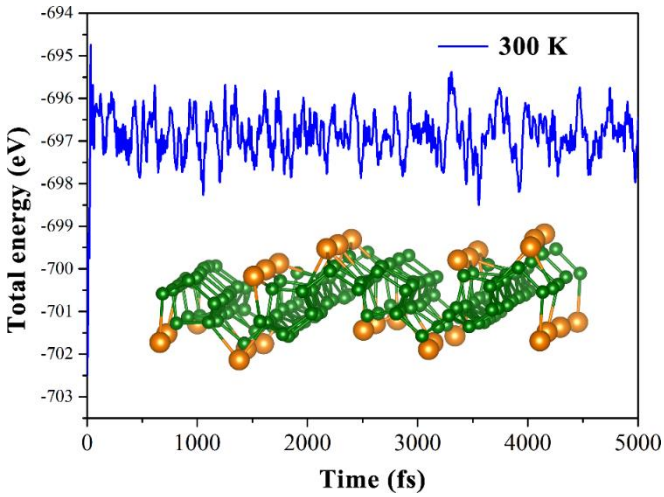

Figure S5 Side view of the snapshots from the molecules dynamics simulation for the monolayer TlP_5. The variation of total energy was recorded during the simulation time of 5 ps, and the temperature was 300 K.

Table S1 The optimized P-P and Tl-P bond lengths in the monolayer TlP_5 ("1L" for short) and bulk, respectively, in comparison to the experimentally verified values (Exp.) for the bulk. The numbers in parentheses count the equivalent P-P bonds in a unit cell, and the corresponding bond locations are marked in **Figure S4**.

	1L TlP_5	Bulk TlP_5	Exp.
	P-P (Å)	P-P (Å)	P-P (Å)
P1(4)	2.243	2.242	2.242
P2(4)	2.218	2.216	2.213
P3(4)	2.27	2.275	2.229
P4(4)	2.238	2.228	2.222
P5(4)	2.227	2.218	2.225
P6(2)	2.174	2.172	2.174
P7(2)	2.157	2.15	2.126
P8(4)	2.187	2.178	2.13
P9(2)	2.203	2.198	2.221
	P-TI(Å)	P-TI(Å)	P-TI(Å)
TI1(4)	3.17	3.03	2.985
TI2(4)	3.01	3.023	3.015
TI3(2)	3.008	2.998	2.986
TI4(2)	3.04	3.089	3.025

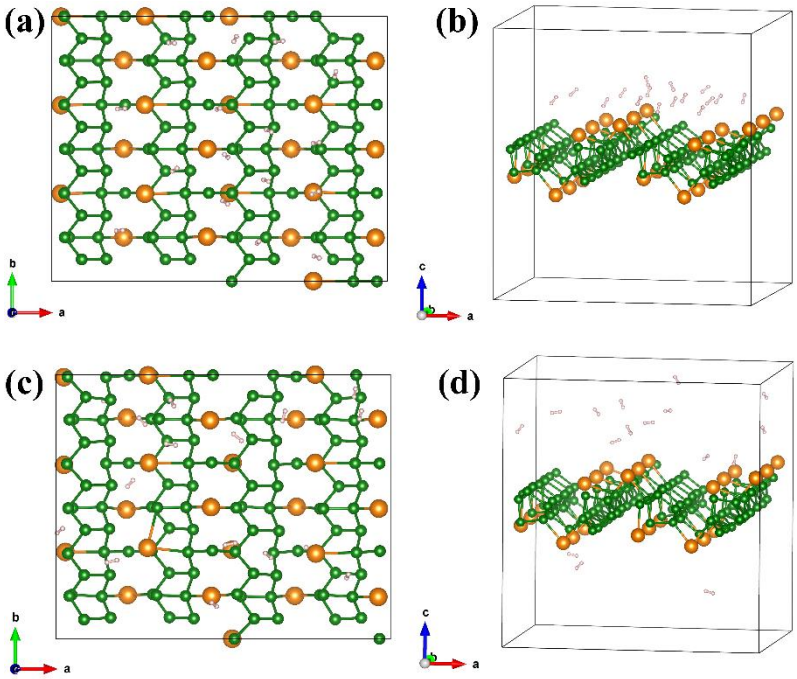

Figure S6 *Ab initio* molecules dynamics simulation for H_2 on monolayer TlP_5. The optimized (a) top view and (b) side view of sixteen H_2 on monolayer TlP_5 at 0K; (c) top view and (d) side view of sixteen H_2 on monolayer TlP_5 during the simulation time of 5 *ps* at 300 K.

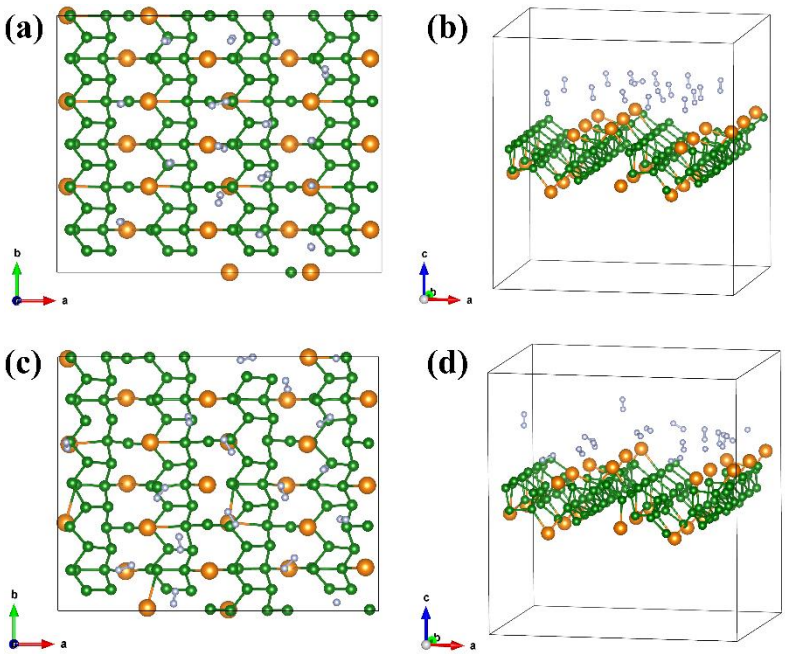

Figure S7 *Ab initio* molecules dynamics simulation for N_2 on monolayer TlP_5. The optimized (a) top view and (b) side view of sixteen N_2 on monolayer TlP_5 at 0K; (c) top view and (d) side view of sixteen N_2 on monolayer TlP_5 during the simulation time of 5 *ps* at 300 K.

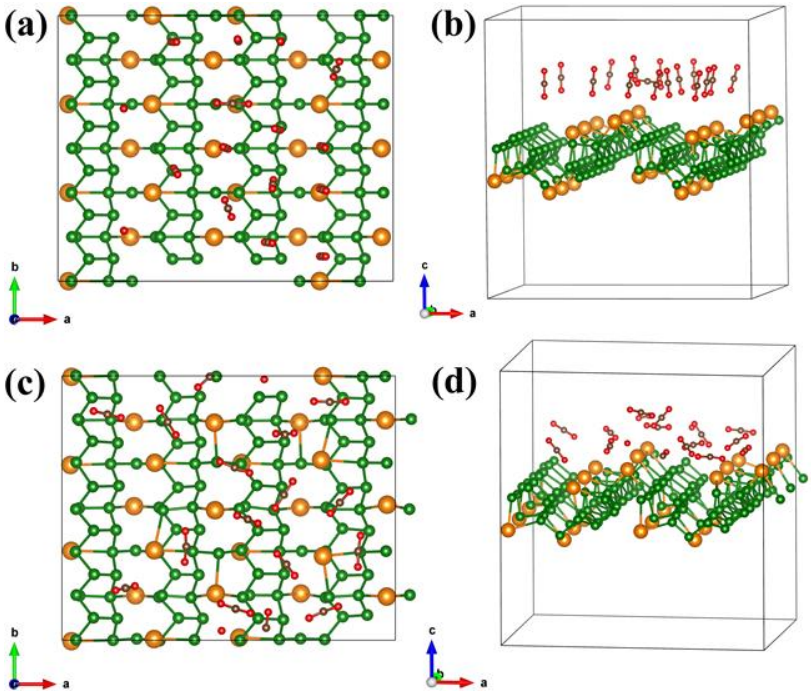

Figure S8 *Ab initio* molecules dynamics simulation for CO_2 on monolayer TlP_5. The optimized (a) top view and (b) side view of sixteen CO_2 on monolayer TlP_5 at 0K; (c) top view and (d) side view of sixteen CO_2 on monolayer TlP_5 during the simulation time of 5 *ps* at 300 K.

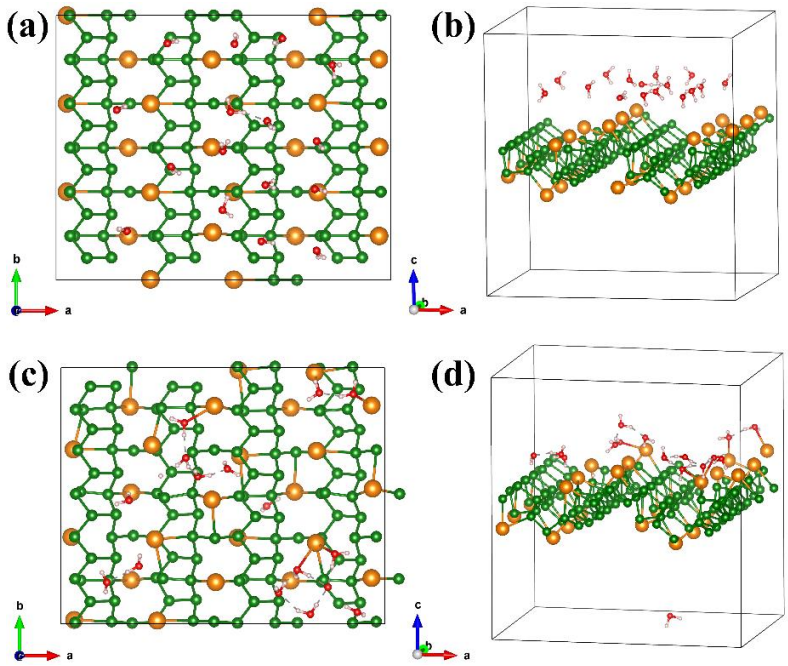

Figure S9 *Ab initio* molecules dynamics simulation for H_2O on monolayer TlP_5. The optimized (a) top view and (b) side view of sixteen H_2O on monolayer TlP_5 at 0K; (c) top view and (d) side view of sixteen H_2O on monolayer TlP_5 during the simulation time of 5 *ps* at 300 K.

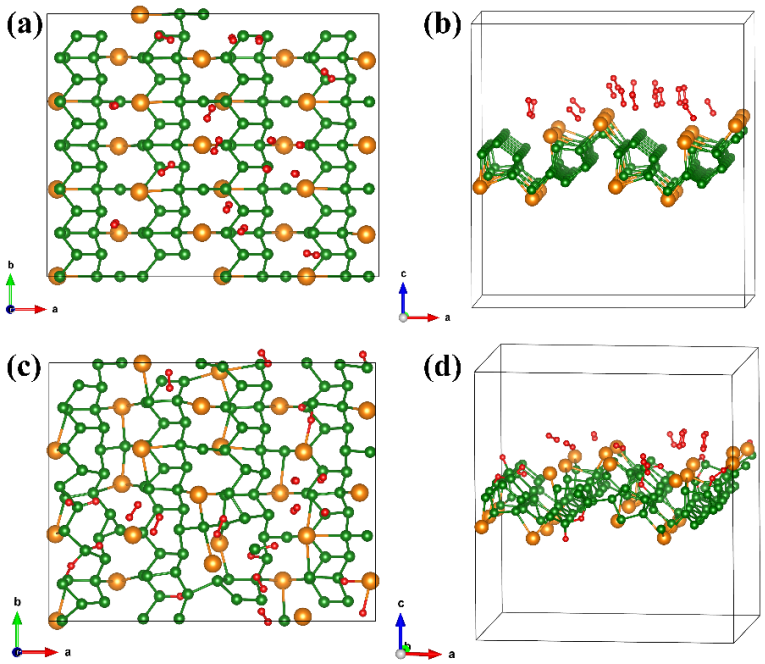

Figure S10 *Ab initio* molecules dynamics simulation for O_2 on monolayer TlP_5. The optimized (a) top view and (b) side view of sixteen O_2 on monolayer TlP_5 at 0K; (c) top view and (d) side view of sixteen O_2 on monolayer TlP_5 during the simulation time of 5 *ps* at 300 K.

The optimized lattice constants of *n*L (*n*=1, 2, 3, 4, 5) TlP_5 and bulk are listed in Table S2, with reference to experimental values. The optimized lattice parameters of monolayer TlP_5 are a =12.35 Å and b = 6.51 Å (note that the a/b here actually correspond to the c/a directions in bulk). Upon the increase in the number of layers, the lattice constants vary very little, indicating a relatively weak interlayer coupling in the TlP_5 system.

Table S2 The optimized lattice constants (a/b/c) in TlP_5 monolayer (1L), bilayer (2L), tri-layer (3L), four-layer (4L), five-layer (5L) and bulk, respectively, in comparison to the experimental values (Exp.) for the bulk.

Lattice constant	1L	2L	3L	4L	5L	Bulk	Exp.[2]
a/Å	12.35	12.27	12.26	12.26	12.25	6.48	6.46
b/Å	6.51	6.49	6.49	6.48	6.48	7.01	6.92
c/Å	--	--	--	--	--	12.24	12.12

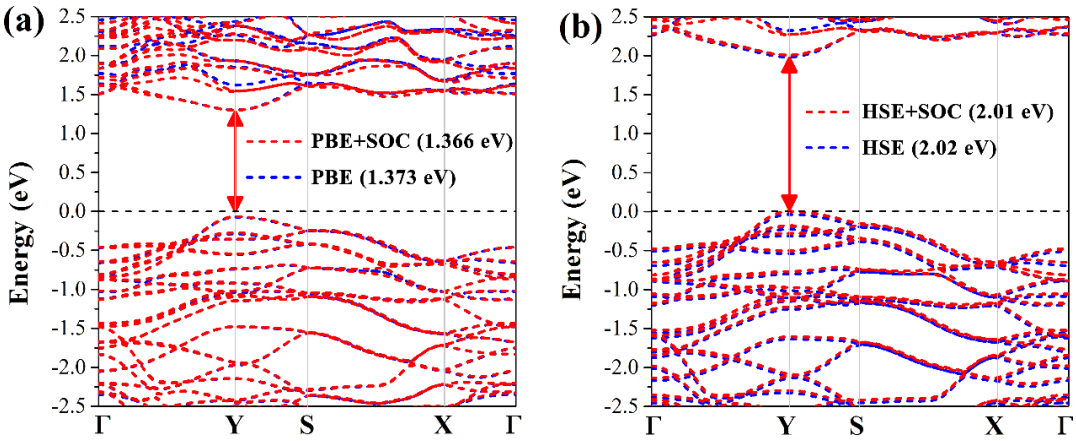

Figure S11 (a) Band structures of monolayer TlP_5 calculated using the PBE functional, either with or without considering the effect of spin orbit coupling (SOC). (b) Band structures of monolayer TlP_5 calculated using the screened HSE06 hybrid functional, either with or without considering the effect of SOC.

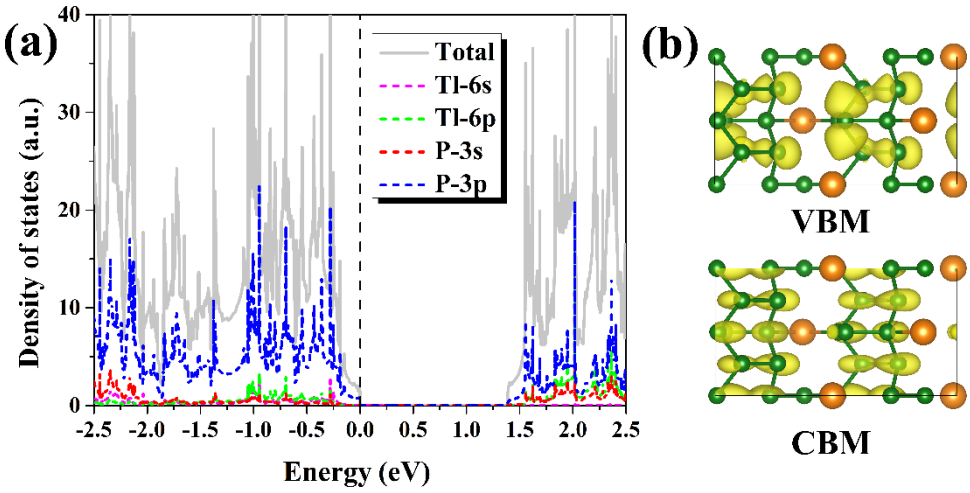

Figure S12 (a) Projected density of states of monolayer TlP_5. (b) Isosurfaces of partial charge densities corresponding to the VBM and CBM of monolayer TlP_5.

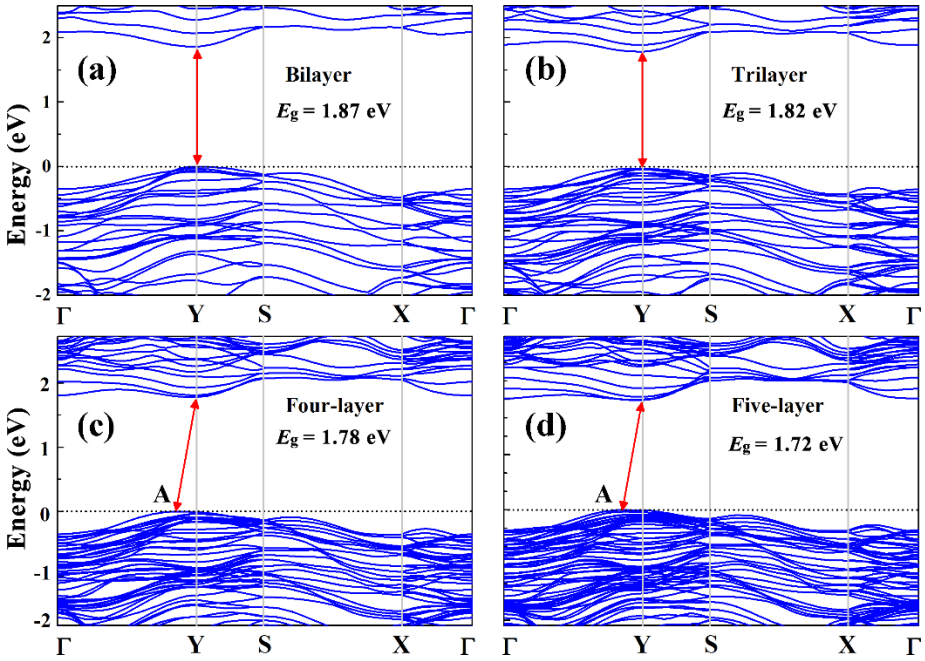

Figure S13 Electronic band structures of 2D TlP_5 with varying number of layers, calculated using the screened HSE06 hybrid functional: (a) bilayer; (b) trilayer; (c) four-layer; and (d) five-layer.

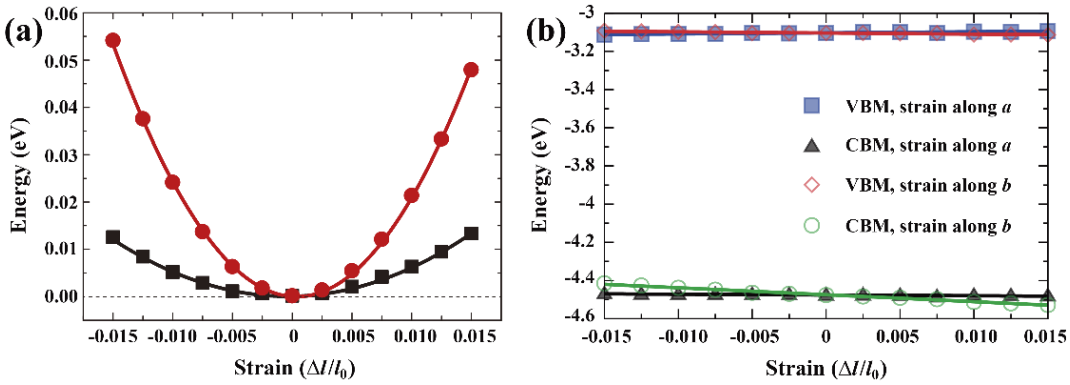

Figure S14 (a) The relationship between total energy and the applied strain δ along the *a* and *b* directions of monolayer TlP_5. The quadratic data fitting gives the in-plane stiffness of 2D structures. Black and red curves show the in-plane stiffness along the *a* and *b* directions of monolayer TlP_5, respectively. (b) The shift of VBMs and CBMs for monolayer TlP_5 with respect to the vacuum energy, as a function of the applied strain along either the *a* or the *b* direction. The linear fit of the data yields the deformation potential constant.

Table S3 The carrier mobilities μ_{2D} ($\times 10^3$ cm^2 V^{-1}s^{-1}) and energy bang gaps (eV, calculated at the HSE06 level) of phosphorene and their derivatives for comparison (only the monolayer is considered). The symbols *d* and *i* represent direct and indirect band gaps, respectively.

	Direction	TlP_5	Phosphorene[3]	Hittorfene[1]	InP_3[4]	GeP_3[5]	CaP_3[6]	SnP_3[7]
Electron	*x*	5.24	1.10~1.14	0.50	0.54	0.04	19.9	0.19
	y	13.96	0.08	0.43	1.92	0.07	1.75	0.21
Hole	*x*	7.56	0.64~0.70	0.31	0.006	0.014(0.35)	0.08	0.17
	y	1.51	10~26	7.68	0.05	0.19(2.36)	0.78	0.36
Band gap		2.02(*d*)	1.51(*d*)	2.5(*d*)	1.14(*i*)	0.55(*i*)	1.15(*d*)	0.72(*i*)

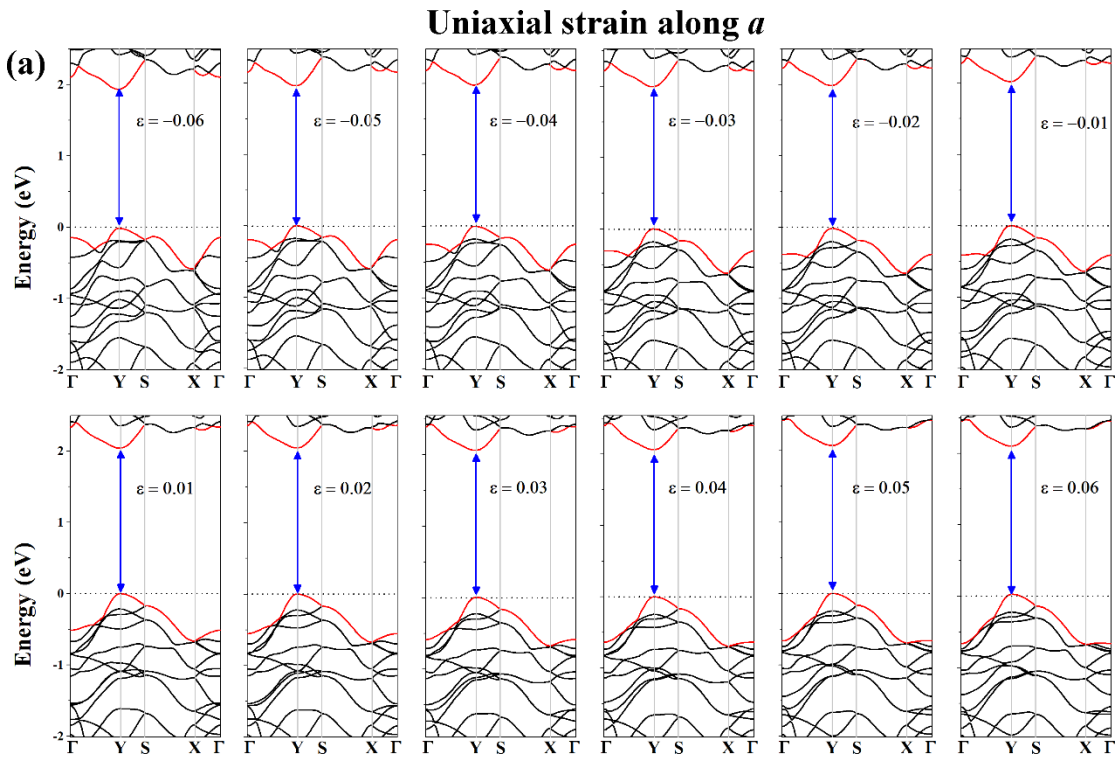

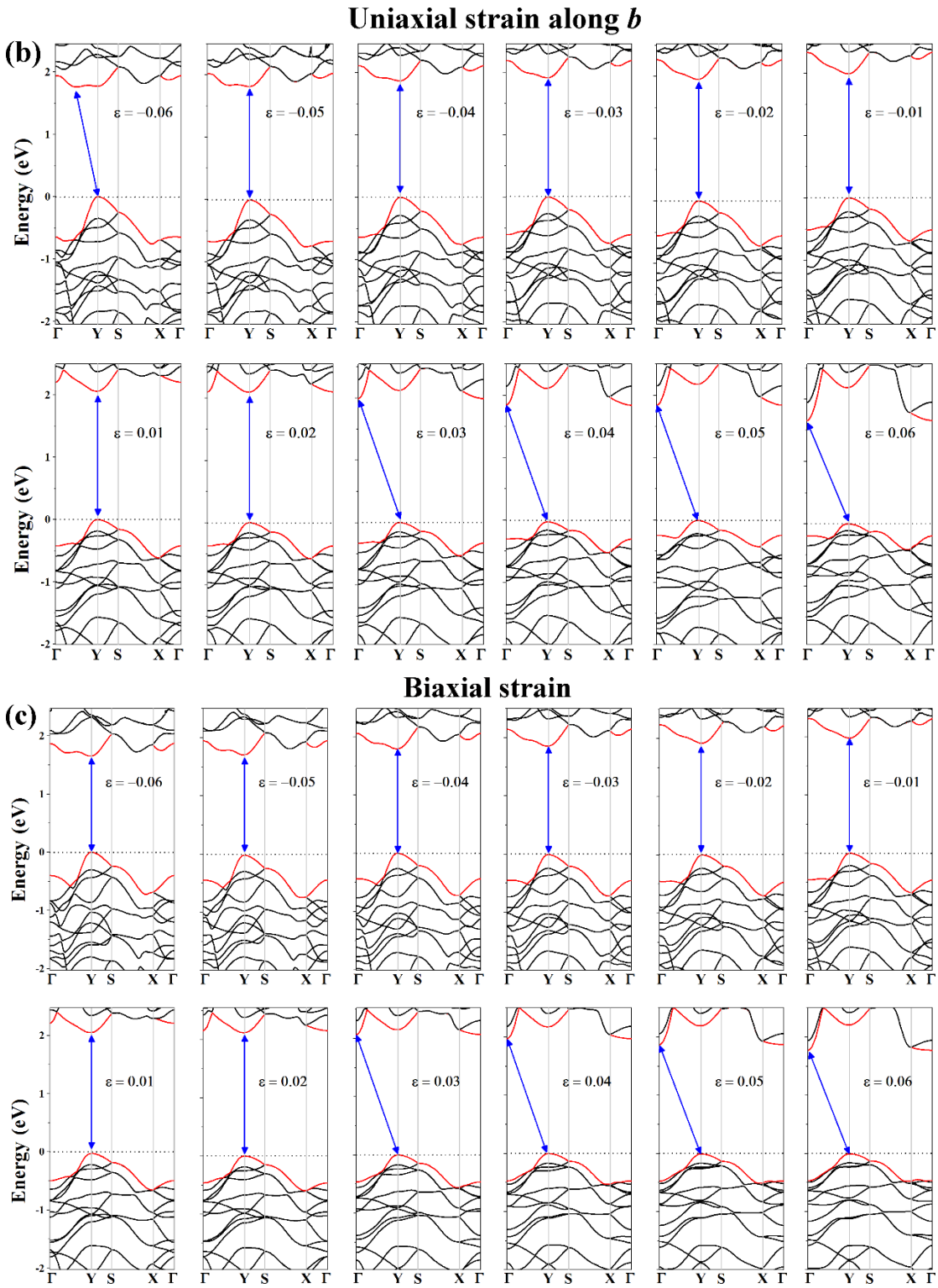

Figure S15 Electronic band structures of monolayer TlP_5 under various strain situations, calculated using the HSE06 functional. The applied strains are (a) uniaxial strain along *a*-axis; (b) uniaxial strain along *b*-axis (b); and (c) biaxial along both *a* and *b*.

REFRENCES

(1) Schusteritsch, G.; Uhrin, M.; Pickard, C. J. Single-Layered Hittorf's Phosphorus: A Wide-Bandgap High Mobility 2D Material. *Nano Letters* **2016**, *16* (5), 2975–2980.

(2) Olofsson, O.; Gullman, J.; Søtofte, I.; Beronius, P.; Engebretsen, J. E.; Ehrenberg, L. The Crystal Structure of TlP5. *Acta Chemica Scandinavica* **1971**, *25*, 1327–1337.

(3) Qiao, J.; Kong, X.; Hu, Z.-X.; Yang, F.; Ji, W. High-Mobility Transport Anisotropy and Linear Dichroism in Few-Layer Black Phosphorus. *Nature Communications* **2014**, *5* (1).

(4) Miao, N.; Xu, B.; Bristowe, N. C.; Zhou, J.; Sun, Z. Tunable Magnetism and Extraordinary Sunlight Absorbance in Indium Triphosphide Monolayer. *J. Am. Chem. Soc.* **2017**, *139* (32), 11125–11131.

(5) Jing, Y.; Ma, Y.; Li, Y.; Heine, T. GeP_3: A Small Indirect Band Gap 2D Crystal with High Carrier Mobility and Strong Interlayer Quantum Confinement. *Nano Letters* **2017**, *17* (3), 1833–1838.

(6) Lu, N.; Zhuo, Z.; Guo, H.; Wu, P.; Fa, W.; Wu, X.; Zeng, X. C. CaP_3: A New Two-Dimensional Functional Material with Desirable Band Gap and Ultrahigh Carrier Mobility. *The Journal of Physical Chemistry Letters* **2018**, *9* (7), 1728–1733.

(7) Sun, S.; Meng, F.; Wang, H.; Wang, H.; Ni, Y. Novel Two-Dimensional Semiconductor SnP_3: High Stability, Tunable Bandgaps and High Carrier Mobility Explored Using First-Principles Calculations. *Journal of Materials Chemistry A* **2018**, *6* (25), 11890–11897.